

# Chemical Science

Volume 15  
Number 10  
14 March 2024  
Pages 3395–3770

[rsc.li/chemical-science](https://rsc.li/chemical-science)



ISSN 2041-6539

**EDGE ARTICLE**

Paul M. Donaldson *et al.*  
Laser induced temperature-jump time resolved IR  
spectroscopy of zeolites

Cite this: *Chem. Sci.*, 2024, 15, 3453

All publication charges for this article have been paid for by the Royal Society of Chemistry

# Laser induced temperature-jump time resolved IR spectroscopy of zeolites†

Alexander P. Hawkins,<sup>a</sup> Amy E. Edmeades,<sup>a</sup> Christopher D. M. Hutchison,<sup>a</sup> Michael Towrie,<sup>a</sup> Russell F. Howe,<sup>b</sup> Gregory M. Greetham<sup>a</sup> and Paul M. Donaldson<sup>\*a</sup>

Combining pulsed laser heating and time-resolved infrared (TR-IR) absorption spectroscopy provides a means of initiating and studying thermally activated chemical reactions and diffusion processes in heterogeneous catalysts on timescales from nanoseconds to seconds. To this end, we investigated single pulse and burst laser heating in zeolite catalysts under realistic conditions using TR-IR spectroscopy. 1 ns, 70  $\mu$ J, 2.8  $\mu$ m laser pulses from a Nd:YAG-pumped optical parametric oscillator were observed to induce temperature-jumps (T-jumps) in zeolite pellets in nanoseconds, with the sample cooling over 1–3 ms. By adopting a tightly focused beam geometry, T-jumps as large as 145 °C from the starting temperature were achieved, demonstrated through comparison of the TR-IR spectra with temperature dependent IR absorption spectra and three dimensional heat transfer modelling using realistic experimental parameters. The simulations provide a detailed understanding of the temperature distribution within the sample and its evolution over the cooling period, which we observe to be bi-exponential. These results provide foundations for determining the magnitude of a T-jump in a catalyst/adsorbate system from its absorption spectrum and physical properties, and for applying T-jump TR-IR spectroscopy to the study of reactive chemistry in heterogeneous catalysts.

Received 15th November 2023

Accepted 29th January 2024

DOI: 10.1039/d3sc06128k

rsc.li/chemical-science

## Introduction

Zeolites are aluminosilicate materials whose nanoporous structure leads to wide application as shape-selective catalysts, catalytic supports and separation materials across multiple chemical industry sectors.<sup>1,2</sup> Catalytic activity occurs at either incorporated metal centres<sup>3</sup> or at framework Brønsted acid sites in the case of protonated zeolites.<sup>1</sup> These applications depend on the complex geometric and chemical properties of the zeolite pore network, dictating how molecules adsorb into and diffuse through the material. Studying the chemistry and interactions of molecules in zeolites on timescales relevant to their diffusion and reaction is critical for developing an improved understanding of the many mechanisms of catalysis in these important materials.

The goal of the work in this paper is the development of methods of IR laser spectroscopy that can initiate and probe chemical change in zeolites across timescales of nanoseconds to seconds. Pulsed-laser infrared (IR) absorption spectroscopy allows vibrational spectra to be recorded with a time resolution

as small as femtoseconds,<sup>4,5</sup> allowing the study of dynamical processes such as bond breaking, structural rearrangements and molecular diffusion.<sup>6–9</sup> Dynamical processes are initiated by pulsed-laser excitation and monitored with synchronised, time-resolved spectroscopic probing of the resulting molecular changes. It is common to initiate chemistry by excitation of electronic absorption bands in the UV/visible part of the spectrum, however using a laser to simply heat a sample (temperature-jump, or T-jump spectroscopy) enables thermally activated processes to be studied over multiple decades in time from picoseconds to milliseconds.<sup>10–14</sup> The time for a sample to fall back to its initial temperature is dependent on its thermal properties. Starting with ps–ns heating pulses, elevated temperatures in the millisecond range are possible for solution phase samples, allowing non-equilibrium structural dynamics to be observed,<sup>14–16</sup> with further timescales accessible through more sophisticated laser heater sources.<sup>15</sup>

While IR laser T-jump methods have seen application to solution-phase chemistry<sup>10–19</sup> particularly in the field of biomolecule dynamics,<sup>10–13,16,18,19</sup> time resolved IR T-jump investigations of heterogeneous catalysts are absent in the literature. The use of CW lasers to simply heat zeolites has been explored,<sup>20–22</sup> but the ability to synchronously collect time-resolved spectra on the evolution of the sample was not implemented. Picosecond pulsed-IR investigations of zeolites have demonstrated how the relaxation of excited O–H and O–D

<sup>a</sup>Central Laser Facility, Research Complex at Harwell, STFC Rutherford Appleton Laboratory, Didcot, Oxon, OX11 0QX, UK. E-mail: paul.donaldson@stfc.ac.uk

<sup>b</sup>Department of Chemistry, University of Aberdeen, Aberdeen, AB24 3UE, UK

† Electronic supplementary information (ESI) available. See DOI: <https://doi.org/10.1039/d3sc06128k>



vibrations induces heating of the zeolite framework, and quantified the resulting temperature transients, but considered the heating as an unwanted background to the investigation of vibrational relaxation on picosecond timescales.<sup>23,24</sup> The ability to heat solid materials and monitor their evolution from nanoseconds to seconds with time-resolved IR remains unexplored. In this paper we describe experiments to do exactly this with an approach of pulsed-laser T-jumping and time-resolved IR probing for investigating laser heating in a hydrated commercial H-ZSM-5 zeolite powder. Acid zeolites possess strongly absorbing O–H vibrations at around  $3600\text{ cm}^{-1}$ . These are ideal modes to optically pump and induce the required laser heating. To this end, a Nd:YAG-pumped Optical Parametric Oscillator (OPO) operating in the mid-IR was used. Time resolved multiple probe spectroscopy (TRMPS) with a broadband IR probe<sup>14</sup> was able to access dynamical timescales from nanoseconds to seconds in a single measurement, representing a new approach to investigate fast temperature-related phenomena in zeolites. We demonstrate here time-resolved IR experiments performed in transmission with compressed (pelleted) solid zeolite samples under conditions of controlled gas flow and elevated sample temperature. Classical heat transfer simulations<sup>14,15</sup> of the pumped sample are used to provide insight into the spatial distribution and temporal evolution of heat. We experimentally determine the time-dependent temperature of the laser heated zeolite sample relative to its starting conditions by using the established approach of identifying temperature-dependant modes in the IR spectrum for use as spectroscopic ‘thermometers’. For zeolites, by partially deuterating the samples and probing spectral changes in the  $2500\text{--}3000\text{ cm}^{-1}$  spectral range, we find that the narrow, temperature-sensitive stretch band of deuterated, intrinsic silanol groups makes an excellent ‘thermometer’. Optical scattering from the bright T-jump laser pulse can easily saturate the IR detector used to monitor the probe transmission. Partial deuteration allows  $\nu(\text{OH})$  stretch mode pumping and probing in the separate spectral region of mainly  $\nu(\text{OD})$  stretch modes.

Compared with earlier liquid-phase T-jump studies,<sup>14,15</sup> we find that a significant increase in T-jump magnitude can be gained by tightly focussing the pump beam to radial dimensions of  $\sim 40$  microns in size. An even tighter focussed probe beam then passes through the centre of the excited sample volume. Such tightly focussed ns excitation pulses can cause cavitation and shock waves in liquid sample cells. A significant observation in this work is that zeolites, in the form of free-standing, compressed pellets of microcrystalline particles are robust under such excitation— we observed no evidence of cavitation, shock waves or damage. The lower thermal conductivity and specific heat capacity of zeolites compared to liquid water also means that larger T-jumps for a given energy input are achieved. Comparison of time resolved silanol  $\nu(\text{OD})$  stretch shifts with steady-state Fourier transform IR (FT-IR) spectra confirm that single laser pulse T-jumps with magnitudes of up to  $+145\text{ }^{\circ}\text{C}$  above starting temperature are achieved with lifetimes into the millisecond time range. Allowing the Nd:YAG OPO pump laser to release repeated bursts of heating pulses spaced 1 ms apart achieves even higher levels of heating.

These results establish an experimental and conceptual framework for the measurement and analysis of T-jumps which we expect to be applicable to a wide variety of zeolite-adsorbate systems.

## Experimental

### Samples

ZSM-5 was sourced from Zeolyst (CBV5524G) in the  $\text{NH}_4$ -ZSM-5 powder form and converted to H-ZSM-5 by calcination in static air at  $550\text{ }^{\circ}\text{C}$  for 24 hours. X-ray fluorescence characterisation of the calcined powder confirmed a nominal framework Si:Al ratio of 25:1.

All spectroscopic measurements were performed in transmission geometry on self-supporting zeolite pellets of  $70\text{--}150\text{ }\mu\text{m}$  thickness prepared from  $7\text{--}15\text{ mg}$  of powdered sample held at 1 ton for 1 minute in a pellet press (Specac). Pellets were held in a heated spectroscopy cell with gas-flow capability (Linkam FTIR600) and sample temperature controlled by the sample being in direct contact with a cell heater block held between (but not in contact with) two  $\text{CaF}_2$  windows. A centrally located 4 mm hole in the heater block allowed passage of light through the pellet. For a given heater block temperature set-point, the free-standing portion of the zeolite had a static thermal gradient, with the sample coolest in the middle (farthest from the heater block). This gradient was measured by thermal imaging of the sample.<sup>25</sup>

Measurements were carried out at 1 atmosphere under flowing  $\text{N}_2$  (liquid  $\text{N}_2$  boil-off) with sample hydration and deuteration achieved by sparging controlled flows of  $\text{N}_2$  through a Drechsel flask containing a 20% solution of  $\text{D}_2\text{O}$  in  $\text{H}_2\text{O}$  (referred to as  $\text{HOD}/\text{H}_2\text{O}$  below for brevity). A schematic of the gas flow apparatus is shown in the ESI Section 1.† FT-IR spectra were collected using a Bruker Tensor spectrometer operated at  $4\text{ cm}^{-1}$  spectral resolution.

### Time-resolved spectroscopy

T-Jump spectroscopy was carried out at the Rutherford-Appleton Laboratory Ultra facility using a variation on the TRMPS technique.<sup>14,26</sup> The experiment is shown in Fig. 1. To adequately cover the  $\nu(\text{CH})$  and  $\nu(\text{OD})$  modes of the vibrational spectrum, probe pulses centred at *ca.*  $2700\text{ cm}^{-1}$  with a useable bandwidth  $>500\text{ cm}^{-1}$  and an energy of  $1\text{--}2\text{ }\mu\text{J}$  per pulse were generated at 10 kHz by difference frequency mixing the output of an Optical Parametric Amplifier (OPA, Light Conversion TOPAS) pumped by 5 W of 800 nm light sourced from a 20 W, 50 fs Ti:Sapphire amplifier system (Coherent Legend Elite Duo). Pump pulses of  $\sim 110\text{ }\mu\text{J}$  energy and  $<1.5\text{ ns}$  duration centred at  $3600\text{ cm}^{-1}$  were generated using 2 mJ of light from a Nd:YAG (BrightSolutions Wedge, 1 kHz, 4 mJ) pumping a home-built OPO based on periodically poled lithium niobate (PPLN, Covesion) heated to  $75\text{ }^{\circ}\text{C}$  to give an OPO output of  $3600\text{ cm}^{-1}$  with a pulse duration  $<1.5\text{ ns}$ .<sup>14</sup> In Fig. 1, the pump laser is synchronised to the probe laser and operated at repetition rates from 2 Hz to 1 kHz. High-voltage Q-switch noise from the pump laser coupling into the IR detection system is subtracted using



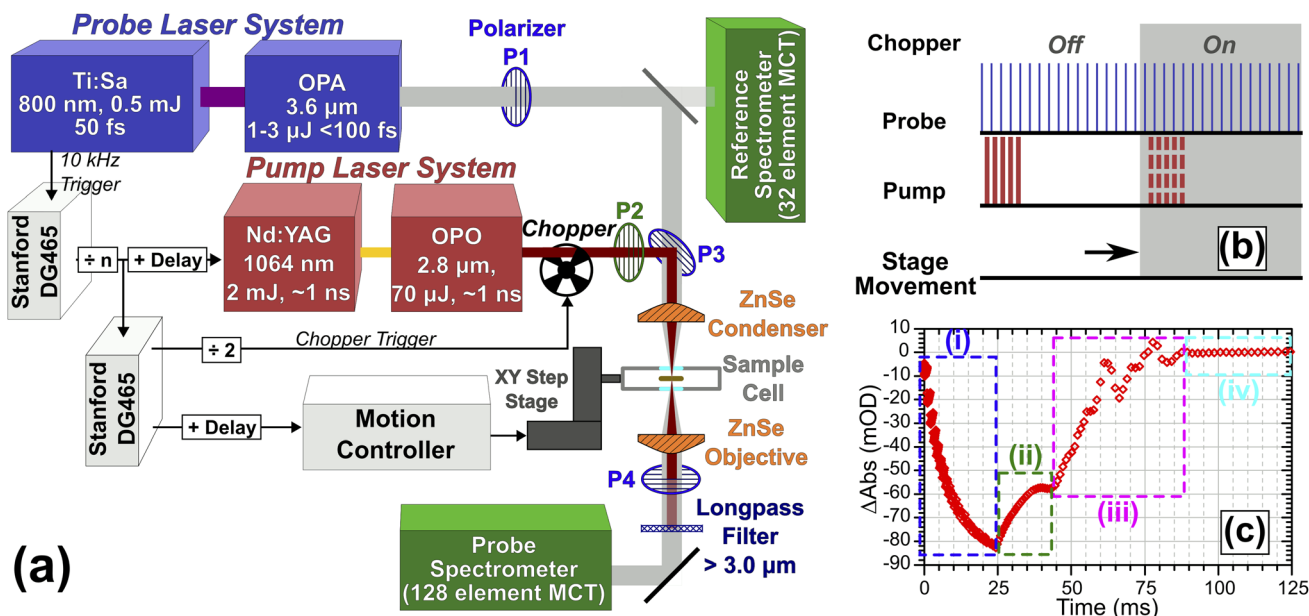


**Fig. 1** (a) Experimental layout showing optical and sample environment components for time-resolved IR spectroscopy T-jump measurements. (b) Pulse scheme and synchronised sample movement for TRMPS technique. (c) Spectral intensity at 2750  $\text{cm}^{-1}$  vs. time for HOD/H<sub>2</sub>O in ZSM-5 excited with  $25 \times 70 \mu\text{J}$  pump pulses showing effects of (i) sample excitation, (ii) decay, (iii) noise from stage movement and (iv) return to unpumped state post-movement.

a chopper operating at half the pump repetition rate, giving a ‘pump-off’ dataset for each entire TRMPS probe sequence.<sup>14</sup> The longest TRMPS time delay measurable is then half the pump pulse period. The 10 kHz probing gives multiple probe pulses spaced by 100  $\mu\text{s}$ . To achieve sub-100  $\mu\text{s}$  time resolution on the first probe pulse of the sequence, the pump–probe pulse timing is controlled by triggering the Nd:YAG Q-switch at a fixed delay set by a computer controlled pulse delay generator (Stanford DG465), which could also trigger the Nd:YAG laser to make bursts of pulses, each burst treated like a single pump event. For the data in this paper, TRMPS spectra for a given electronic delay were averaged for 30–60 seconds. Further details regarding the triggering of the chopper, sample stage movement and pump bursts are described in ESI Section 2.†

The pump and probe beams were orthogonally polarised and combined collinearly on a wire grid polariser (P3 in Fig. 1), then focused onto the sample using a 12.7 mm focal length ZnSe asphere (Thorlabs). The profiles and divergence characteristics of the focussed beams were examined using a microbolometer camera at the focal plane (see ESI Section 3.†). An accurate characterisation was critical for simulations. The average FWHM size of the pump and probe at the focal plane were  $36 \pm 1.4$  and  $21.5 \pm 1 \mu\text{m}$  respectively. Pulse energies incident on the sample were  $71 \pm 5 \mu\text{J}$  (pump) and  $<0.5 \mu\text{J}$  (probe). After the sample, the beams were re-collimated with a second ZnSe asphere. Residual/scattered pump light was rejected with a long-pass filter. A grating spectrometer dispersed the probe light onto a 128-pixel HgCdTe detector (Infrared Associates) with  $\sim 4 \text{ cm}^{-1}$  resolution per-pixel. IR spectral intensities were digitised shot-by-shot (Infrared Development Systems FPAS) and correlated against simultaneous probe reference intensity

measurements recorded using a small amount of pre-sample probe light sent to a separate spectrometer/detection system to correct for intensity fluctuations using a method similar to that of Feng *et al.*<sup>27</sup>

Spectra were recorded using one of two different measurement schemes. In the first, the sample was held stationary and the pump laser triggered at 20 Hz (chopped to 10 Hz), giving a data collection rate of 10 measurements per second and a 50 ms spectral collection window per measurement due to the need to chop the pump beam. To allow measurement of samples not fully returning to equilibrium conditions in  $<50$  ms, the sample was mounted on a motorised XY translation stage (two Newport XMS series stages, see ESI Section 2.†) which performed a triggered 200  $\mu\text{m}$  step movement of the sample in  $<50$  ms at the end of each measurement, ensuring that each T-jump occurred from an unpumped region of the sample. These step measurements were collected at a rate of 4 measurements per second, giving a 20–40 ms time window stationary interval post pumping while allowing for the movement time of the XY translation stage.

## Results and discussion

In order to understand the time-resolved T-jump data it is useful to first assign the features present in the steady-state FTIR spectra. The IR spectrum of hydrated ZSM-5 is well studied<sup>28–31</sup> and Fig. 2 illustrates how the spectrum of the partially deuterium-exchanged zeolite changes across the temperature range investigated. The sharp feature at 2760  $\text{cm}^{-1}$  corresponds to  $\nu(\text{SiOD})$  modes of silanol groups at the crystal exterior and in internal defects. It is present at all temperatures.

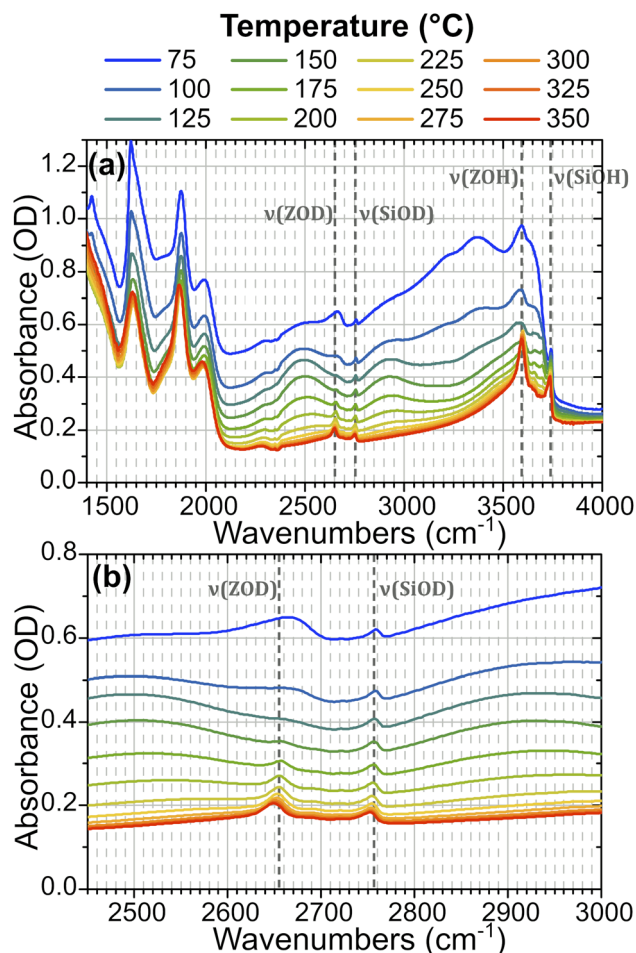


Fig. 2 IR absorption (FTIR) spectra from 1400–4000  $\text{cm}^{-1}$  of ZSM-5 held in flowing HOD/ $\text{H}_2\text{O}$  vapour at indicated temperatures showing (a) all features and (b) the detection range used in the time-resolved spectroscopy. The location of  $\nu(\text{SiOH})$  silanol modes, free  $\nu(\text{ZOH})$  Brønsted acid modes and their deuterated equivalents are highlighted.

The equivalent  $\nu(\text{SiOH})$  mode is visible at  $3750 \text{ cm}^{-1}$ . Above  $125 \text{ }^\circ\text{C}$ , the free  $\nu(\text{OH})$  Brønsted acid site band is visible at  $3590 \text{ cm}^{-1}$ , and the equivalent  $\nu(\text{OD})$  band at  $2655 \text{ cm}^{-1}$ . We refer to these bands as  $\nu(\text{ZOH})$  and  $\nu(\text{ZOD})$  respectively. Hydrogen bonding of ZOH with one or two adsorbed water molecules results in a substantial broadening, structuring and red shifting of the  $\nu(\text{ZOH})$  band.<sup>29,32,33</sup> This creates a broad doublet peaking at *ca.*  $2900 \text{ cm}^{-1}$  and *ca.*  $2500 \text{ cm}^{-1}$ . We refer to this band as  $\nu(\text{ZOH}\cdots(\text{OH}_2)_{n=1,2})$  but note that only the  $2900 \text{ cm}^{-1}$  component of it is fully visible within the spectral range examined in the time-resolved experiments. The corresponding  $\nu(\text{ZOD}\cdots(\text{OH}_2)_{n=1,2})$  band or bands are obscured by the zeolite lattice bands below  $2100 \text{ cm}^{-1}$ . Below  $125 \text{ }^\circ\text{C}$  the spectrum shifts in shape towards the form associated with water clusters with  $>2\text{H}_2\text{O}$  molecules per Brønsted acid site, referred to as  $\text{ZO}^-\cdots\text{H}^+(\text{H}_2\text{O})_{n>2}$ .<sup>28,31,34</sup> Note also that at higher water coverages (lower temperatures)  $\nu(\text{OH})/\nu(\text{OD})$  bands due to weakly hydrogen bonded (terminal) OH/OD groups in hydrogen bonded clusters occur at frequencies close to those of ZOH and ZOD. The weak peak at  $2705 \text{ cm}^{-1}$  at high temperatures is due

to a small population of deuterium exchanged extra-framework aluminium hydroxide species within the pore network, a feature common in commercial zeolite materials.<sup>35,36</sup>

Fig. 3 shows FTIR difference spectra centred on the time-resolved experiment region of hydrated ZSM-5 on heating from initial temperatures of  $100 \text{ }^\circ\text{C}$  (a) and  $175 \text{ }^\circ\text{C}$  (b). The spectra were collected as a continuous temperature ramp ( $2 \text{ }^\circ\text{C}$  per minute). We define the temperature difference  $\Delta T = T_{\text{ramp}} - T_{\text{init}}$ .

Removal of Brønsted site-associated hydrogen-bonded water results in negative intensity changes in the difference spectra in this region. At small  $\Delta T$  values for the  $100 \text{ }^\circ\text{C}$   $T_{\text{init}}$  sample it is mostly clustered water  $\text{ZO}^-\cdots\text{H}^+(\text{H}_2\text{O})_{n>2}$  which is removed, giving a flatter difference spectrum (Fig. 3(a)). With increasing  $\Delta T$ , at  $T_{\text{init}} = 100 \text{ }^\circ\text{C}$ , the removal of  $\text{ZOH}\cdots(\text{OH}_2)_{n=1,2}$  water molecules hydrogen-bonded to the protonated Brønsted sites results in broad negative features at  $\sim 2900$  and  $2500 \text{ cm}^{-1}$  in the difference spectra due to loss of the hydrogen bonds. Superimposed on these broad negative features is a positive feature at  $2660 \text{ cm}^{-1}$  due to Brønsted acid ZOD groups recovered by the water loss. Note that the shape of this feature is distorted by the temperature dependent frequency shift well known for zeolite hydroxyl groups.<sup>37,38</sup> There is also a negative feature at the SiOD frequency ( $2760 \text{ cm}^{-1}$ ) which increases with increasing temperature. This is due to the fact that the absorption coefficient for  $\nu(\text{SiOD})$  vibrations decreases markedly with increasing temperature, as discussed further below. For  $T_{\text{init}} = 175 \text{ }^\circ\text{C}$  the sample contains no clustered water  $\text{ZO}^-\cdots\text{H}^+(\text{H}_2\text{O})_{n>2}$  and the removal of

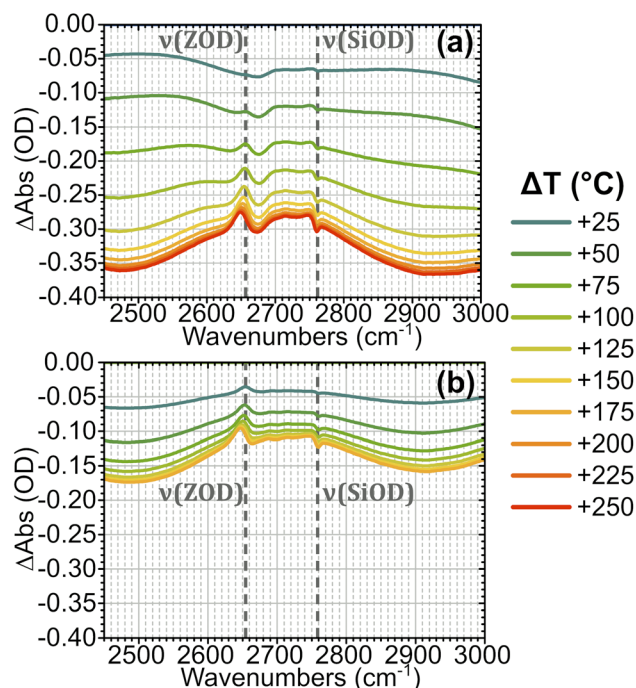


Fig. 3 FTIR temperature ramp difference spectra of ZSM-5 in flowing HOD/ $\text{H}_2\text{O}$  vapour on heating relative to  $100 \text{ }^\circ\text{C}$  (a) and  $175 \text{ }^\circ\text{C}$  (b) at the indicated  $\Delta T$  values. The corresponding difference spectra relative to other temperatures are shown in the ESI, Section 4.† The location of  $\nu(\text{SiOD})$  silanol modes and  $\nu(\text{ZOD})$  Brønsted acid modes are highlighted.



ZOH $\cdots$ (OH $_2$ ) $_{n=1,2}$  water proceeds for all values of  $\Delta T$  (Fig. 3(b)). Intensity changes are weaker in the  $T_{\text{init}} = 175^\circ\text{C}$  spectrum for the same  $\Delta T$  value due to the lower initial population of water.

Fig. 4 shows T-jump transient IR spectra across a time range of over seven orders of magnitude for a ZSM-5 pellet held in the presence of dilute HOD/H $_2$ O vapour and heated with a ns IR laser pulse at a 10 Hz repetition rate. Initial temperatures ( $T_{\text{init}}$ ) of 100 and 175  $^\circ\text{C}$  are chosen for discussion as they are representative of the overall trends in sample response, and allow a direct comparison with the temperature ramp FTIR data in Fig. 3. Samples were measured at 8 initial temperatures from 80–300  $^\circ\text{C}$ . Transient IR spectra for these additional  $T_{\text{init}}$  values are shown in ESI Section 5.† The plots are difference spectra (in units of optical density) relative to the unpumped state of the sample. Negative signals correspond to an increase in transmission (decrease in absorption), positive signals correspond to a decrease in transmission (increase in absorption).

The spectral changes observed in the T-jump transient spectra of Fig. 4 are consistent with the sample undergoing rapid heating due to absorption of the pump laser light, and qualitatively match the form of difference spectra taken by FT-IR for increasing temperature in Fig. 3. For the sample held initially at 100  $^\circ\text{C}$  (Fig. 4(a)) the loss of adsorbed water is seen as a negative baseline shift due to loss of water clusters, and the growth of two negative features at  $\sim 2900\text{ cm}^{-1}$  and below

$2500\text{ cm}^{-1}$  due to loss of hydrogen bonded ZOD groups, as discussed for the FT-IR temperature ramp. These negative changes are  $\sim 5\times$  smaller than those seen in the FTIR difference spectra, presumably because in the T-jump experiments the sample begins cooling before desorption reaches equilibrium. The subsequent decline of these negative features indicates that water readsorbs on a time scale of tens of milliseconds. The negative  $\nu(\text{SiOD})$  band indicates a temperature increase due to the pump pulse which can be quantified after appropriate calibration, as discussed below.

The recovery of ZOD groups accompanying loss of hydrogen bonded water which is very evident in the FTIR temperature ramp difference spectra in Fig. 3(a) is scarcely seen in the T-jump difference spectra in Fig. 4(a). This difference between FTIR and T-jump spectra is also seen at an initial temperature of 80  $^\circ\text{C}$  (ESI Fig. S4†). The missing appearance of free Brønsted sites after heating in the transient data may be an indication that the T-jump causes a large population of Brønsted sites ZOD $\cdots$ (OH $_2$ ) $_{n=1,2}$  to immediately become deprotonated, with accompanying formation of D $^+$ (OH $_2$ ) $_{n=1,2}$ . A minimal free ZOD Brønsted population throughout the heating and cooling process would therefore be expected, as is observed in the data. Since the water present in the sample is deuterated to the same level (10%) as the zeolite acid sites, the amount of D  $\rightarrow$  H exchange from deprotonation of ZOD sites will be matched by H  $\rightarrow$  D exchange of ZO $^-$  generated from ZOH sites.

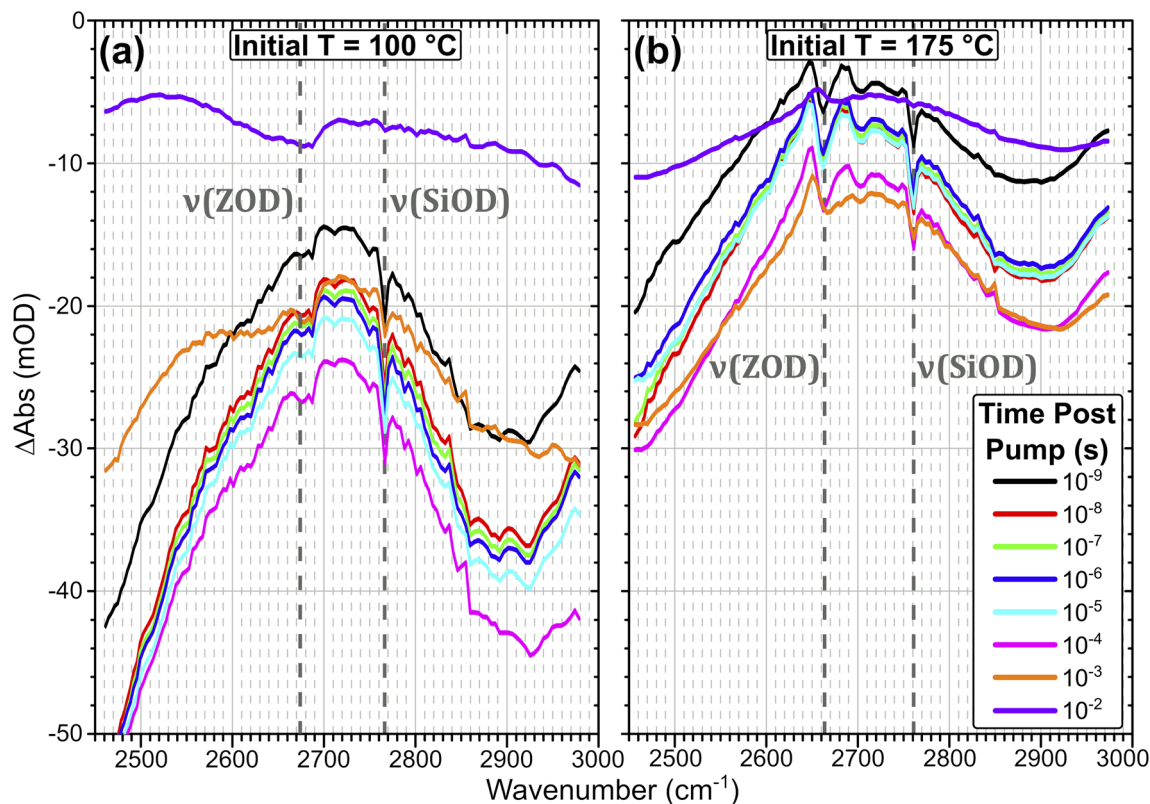


Fig. 4 Time-resolved IR spectral evolution of ZSM-5 in flowing HOD/H $_2$ O vapour at an initial temperature of 100  $^\circ\text{C}$  (a) and 175  $^\circ\text{C}$  (b). Spectra are shown at logarithmic time intervals from  $10^{-9}$ – $10^{-2}$  s following pumping with the 70  $\mu\text{J}$  laser pulse. The  $\nu(\text{SiOD})$  silanol modes and free  $\nu(\text{OD})$  Brønsted acid modes are highlighted.



The sample held initially at 175 °C (Fig. 4(b)) contains no adsorbed water clusters ( $\text{H}_2\text{O}_n$ ,  $n > 1$ ). The difference spectra recorded following the T-jump pulse show the negative bands due to loss of hydrogen bonded ZOD groups, the negative SiOD feature caused by the increased temperature and the expected positive feature due to recovery of free ZOD groups, which is distorted by the temperature dependent frequency shift. The relative contributions of desorption and frequency shift to the  $\nu(\text{OD})$  band can be separated by comparing the FTIR and T-jump data at different temperatures (ESI Section 6†). In ESI Section 7† we plot the decay kinetics of the positive (recovery) and negative (frequency shift) components of the  $\nu(\text{OD})$  band for initial sample temperatures of 175 and 300 °C respectively. At 175 °C the two components decay with different time constants. At 300 °C, where no adsorbed water of any kind is present, the only contribution to the difference spectrum is the temperature dependent frequency shift, and the two components decay synchronously.

Examining the spectral evolution of the data in Fig. 4, the negative features in the spectra associated with water desorption increase from a pump-probe delay of  $t = 0$  to *ca.*  $10^{-4}$ – $10^{-3}$  s, followed by recovery as the sample begins to return to its equilibrium conditions. The shifts of the silanol and free Brønsted ZOD modes due to the heating of the sample evolve on a different timescale to the modes associated with water desorption, evidenced by the water desorption modes persisting in the spectra at  $10^{-2}$  s while these other features are already fully decayed. The kinetics of the silanol and water-associated modes in the spectra at different temperatures are shown in ESI Section 8.† We now turn to establishing the heating and cooling behaviour of the zeolite on laser excitation.

### Heating and cooling of ZSM-5 on laser excitation

To quantify the temperature changes occurring on laser excitation, we explored the effectiveness of the silanol  $\nu(\text{SiOD})$  band as a thermometer. This band shows no interaction with water under the conditions of these experiments, so that variations in its frequency and intensity with temperature provide a way to estimate temperature changes during the T-jump experiments. Variations in the  $\nu(\text{ZOD})$  band in dry zeolites and the  $\nu(\text{CO})$  bands of trifluoroacetic acid have previously been used successfully as thermometers in other studies in the literature.<sup>14,38</sup> Fig. S8(a) in the ESI† shows how the silanol band in ZSM-5 varies with temperature in the FTIR spectra. To remove the contributions to the transient spectra from water desorption, baseline subtraction close to the edges of the  $\nu(\text{SiOD})$  band is applied. Applying this also to FT-IR difference spectra from the same starting temperature allows a relationship between the silanol mode absorbance change and increase in temperature to be established. The  $\nu(\text{SiOD})$  band is observed by FT-IR to shift and weaken as a function of increasing temperature. Frequency shifts alone produce a symmetric derivative in the difference spectra, while an absorbance decrease alone would give a negative peak in the difference spectrum. The combination of a frequency shift to lower frequency and an absorbance decrease gives an asymmetric difference band with an

enhanced negative lobe on the high frequency side. This is illustrated with simulated spectra in ESI Fig. S9.† Fig. 5 shows how the intensity of this negative lobe in difference FTIR spectra can be used to construct a calibration curve. A linear baseline is fitted to the difference spectrum as illustrated in Fig. 5(a) and the baseline subtracted spectra plotted as a function of the temperature difference in Fig. 5(b). The intensity of the negative lobe is a linear function of the temperature difference (Fig. 5(c)). The linear slope of  $1/K$  provides a conversion factor  $K$  used to convert the intensity of the  $\nu(\text{SiOD})$  difference feature to the corresponding change in sample temperature.

$$\Delta T(t) = K \Delta \text{Abs}_{(\text{SiOD})}(t) \quad (1)$$

Values of  $K$  for initial temperatures between 80 and 300 °C are listed in ESI Table S2.† We confirmed that the calibration curves were independent of the water vapour pressure at least up to 300 °C (see Fig. S10†).

From calibration curves constructed we can then estimate temperature changes occurring in the T-jump experiments. Fig. 6 shows temperature–time dependence curves obtained in this way. The accuracy of the estimate is determined by the fit quality used to derive conversion factor  $K$  and the degree of noise in the time-resolved spectra, and is  $\pm 0.5$ – $3.5$  °C for the data presented here. Instantaneous local heating occurs within the 1.5 ns pump pulse duration because vibrationally excited Brønsted sites, water and silanols relax on  $\sim$ sub 200 ps timescales.<sup>23,24</sup> T-jump rise times of  $\sim 4$  ns are observed, slightly greater than the measured pulse duration of the pump laser.<sup>14</sup> This presumably represents the absorbed energy equilibrating from the location of the O–H sites pumped by the laser pulse to the entire framework within each crystallite. Temperatures stabilise after  $3$ – $10 \times 10^{-9}$  s, after which the zeolite remains hot out to the millisecond time range. The magnitude of the T-jump achieved ( $\Delta T_{\text{Max}}$ ) varies depending on starting temperature (Fig. 6 inset). This is due to the varying levels of water in the sample changing the absorbance in the pump region of the spectrum and therefore the amount of energy absorbed from the pump pulse. The source of this effect is demonstrated by the fact that the samples at 250 and 300 °C are both free of adsorbed water and therefore have virtually identical IR spectra (Fig. 2(a) and S4†) and T-jump magnitudes (Fig. 6 inset).  $\Delta T_{\text{Max}}$  peaks at a  $T_{\text{Init}}$  value of 125 °C, below which  $\Delta T_{\text{Max}}$  decreases, despite the pump absorbance of the sample continuing to increase. The source of this behaviour will be considered in more detail below.

The cooling behaviour of the samples was analysed by fitting the temperature curves of Fig. 6. Points earlier than  $10^{-7}$  s were excluded from the fit in order to capture just the cooling. In all cases the data was found to be best represented by a bi-exponential function of the form:

$$\Delta T(t) = \Delta T_{\text{Max}} \left[ A_1 e^{-\frac{t}{\tau_1}} + A_2 e^{-\frac{t}{\tau_2}} \right] \quad (2)$$



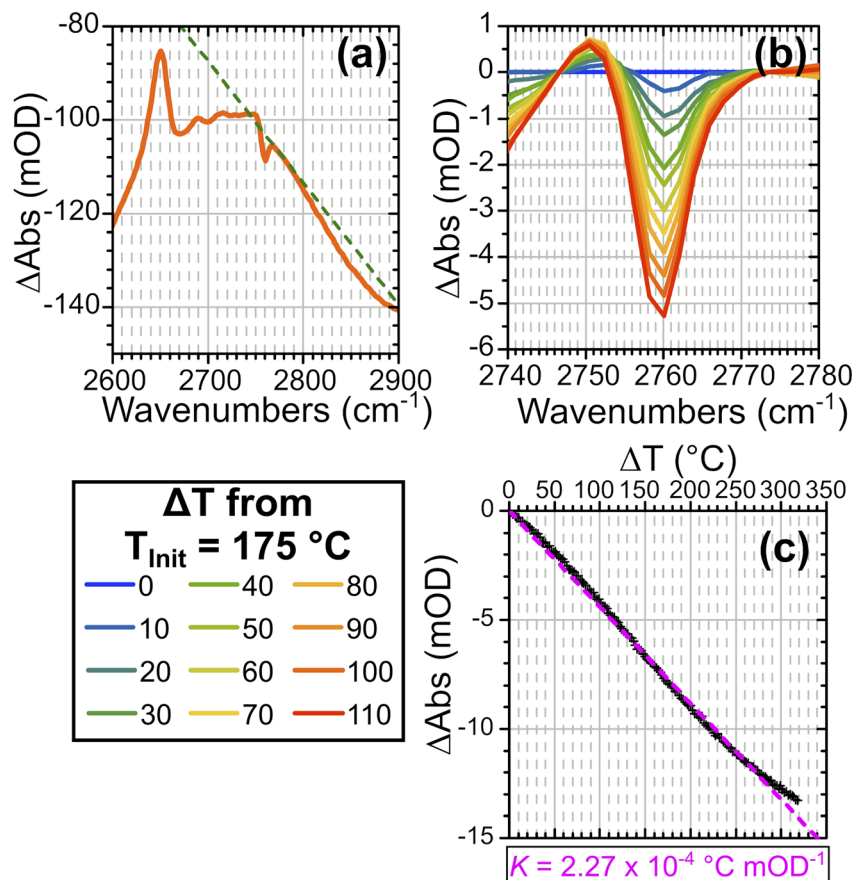


Fig. 5 (a) FTIR difference spectrum of  $\Delta T = 50^\circ\text{C}$  from  $T_{\text{init}} = 175^\circ\text{C}$  showing a linear baseline fit to isolate silanol mode contributions. (b) Comparison of the  $\nu(\text{SiOD})$  feature in baseline subtracted difference spectra at indicated  $\Delta T$  values showing increase in intensity of negative feature with increased  $\Delta T$ . (c) Variation of  $\nu(\text{SiOD})$  negative intensity with  $\Delta T$  showing linear relationship with slope  $1/K$ .

$\tau$  is the time constant for each decay term,  $\Delta T_{\text{Max}}$  the maximum  $\Delta T$  achieved and  $A$  the relative contribution of each term to the overall cooling curve. The fit parameters for each temperature are given in the ESI, Section 10.<sup>†</sup> The first exponential fit to a time constant of *ca.* 0.7 ms accounted for the majority ( $\sim 70\%$ ) of the cooling in each case. The second term, still significant, represents a slower cooling process (time constant *ca.* 6.4 ms). The samples at 80 and 100  $^\circ\text{C}$  exhibit deviations from the trends observed at higher starting temperatures, with slower cooling and larger values of  $\tau$ . To explain why the cooling is bi-exponential, in the next section we examine the temperature distribution within the laser-pumped zeolite sample.

## Heat transfer simulations in laser pumped zeolites

### Simulation method

To understand the time dependent temperature distribution within the ZSM-5 pellets during and following the T-jump laser pulses, the spatial temperature profile and its evolution over time was simulated in three dimensions. Assuming radial symmetry about the excitation laser pulse centre, the model was based on the 2D axisymmetric heat equation in cylindrical

coordinates solved numerically using finite element analysis in Mathematica Version 13.2.<sup>39</sup> The model was solved with logarithmic time steps, to allow high time resolution immediately after the laser pulse, while still following the cooling profile out as far as 1 second. Further details are provided in the ESI, Section 11.<sup>†</sup>

The determination of the simulation input parameters, namely the pump pulse energy, pump and probe spot size, sample absorbance, pellet thickness, sample density, zeolite specific heat capacity ( $C_p$ ) and thermal conductivity ( $\kappa$ ), pump beam quality factor and reflection coefficient, are discussed in ESI Section 12.<sup>†</sup> The effect of the zeolite heat capacity was found to be particularly significant in determining the magnitude of the temperature jump achieved and was modelled using a second-order polynomial derived from fitting experimental data from Lu *et al.*<sup>40</sup> The effect of pump light scattering from the pellet, heat transfer through convection or radiation and the potential temperature-dependence of parameters other than  $C_p$  over the course of the simulation run were not included due to difficulties in quantifying their effects. The effects of asymmetric beam profiles, pump-probe alignment, and the variation of the probed laser spot within the base temperature profile of the zeolite pellet are assumed negligible. These factors are examined in more detail in the ESI, Section 13.<sup>†</sup> Their net effect





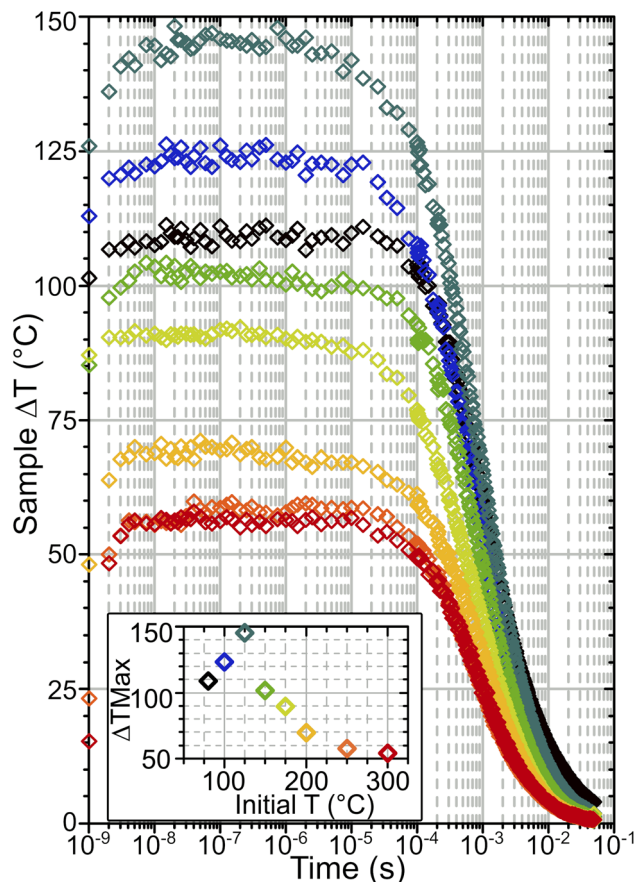


Fig. 6 Sample heating vs. time after ns laser heating for HOD/H<sub>2</sub>O dosed ZSM-5 at different initial temperatures calculated based on changes in silanol mode intensity. The inset plot shows the maximum  $\Delta T$  achieved against initial temperature. The colour scheme of the heating transients corresponds to that in the inset.

is that simulation  $\Delta T$  values are likely to be slightly larger than those observed experimentally, as they represent a more 'ideal' set of conditions.

The output of the simulations are time dependent 2D distributions of temperatures, whereas the temperatures characterised from experimental data represent an average temperature across the probed region. In order to allow comparison between these different types of data, the simulation outputs were converted to a single spatially-averaged

temperature for each time point weighted to account for the variation in probe intensity across the probed region (ESI, Section 14†). Finally, to validate the entire model, T-jumps in water sandwiched between CaF<sub>2</sub> windows, and in free-standing mordenite pellets, were simulated and compared with experiments/simulations reported in the literature<sup>14,15,23</sup> (ESI, Sections 15 and 16†).

### Simulated temperature jumps

The simulated laser pulse heating results in an inhomogeneous temperature distribution in both dimensions of the ZSM-5 pellet (Fig. 7). The radial temperature inhomogeneity is Gaussian, due to the Gaussian profile of the pump laser beam. Temperature inhomogeneity along  $z$  is due to a combination of the absorption of the pump beam as it travels through the sample (resulting in an exponential decay in the amount of energy delivered) and the divergence of the tightly focussed pump beam (resulting in lower intensity at the faces of the pellet than at the pump focus). The highest temperatures in the sample are located in the first half of the pellet depth (see ESI, Section 17†).

Cooling of the sample post-pumping occurred primarily through radial conduction into the unpumped region of the zeolite pellet. Examination of the effects of cooling into the surrounding air (ESI Section 19†) found the contribution of these processes to be minimal. The dominating parameters affecting the rate of radial cooling within the simulation were found to be the pump and probe spot sizes and the thermal conductivity of the zeolite,  $\kappa$ . While the spot size was well characterised by experimental measurements (ESI Section 3†) it was not possible to determine a reasonable estimate for the value of  $\kappa$  from the literature. A range of values were determined empirically by finding the range of  $\kappa$  values for which the fitted time constants fell within the confidence intervals of the experimental cooling curve, with each of the other simulation parameters allowed to vary within their own confidence intervals. This gave a value of  $\kappa = 0.25 \pm 0.1 \text{ W m}^{-1} \text{ K}^{-1}$  for simulations with  $T_{\text{init}}$  from 125–300 °C. The predicted value of  $\kappa$  increases with temperature which is consistent with the results obtained for measurements of thin films,<sup>41–43</sup> although the  $\kappa$  values determined from our experiments are approximately 4 times smaller, possibly indicating the much lower level of thermal contact between crystallites than in a pure film. It was

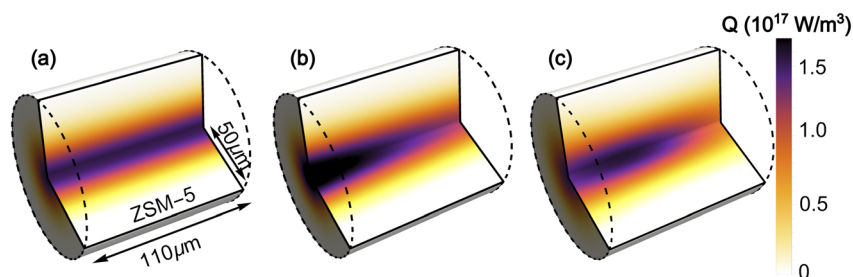


Fig. 7 3D distribution of heat supplied by the pump laser in heat transfer simulations showing in sequence (a) a Gaussian pump beam passing unattenuated through the sample (b) the added effect of attenuation of the pump as it passes through the sample (c) added effect of the divergence of the pump beam.



not possible to derive a value for the thermal conductivity that produced cooling behaviour consistent with the experimental observations at 80 and 100 °C, indicating that at these temperatures there are additional effects from adsorbed water that the simulations do not account for. This results in a deviation of the experimental and simulated T-jump results at low temperatures, which is considered in more detail below. The derived values for  $\kappa$  are given in Table S3 in the ESI (Section 10).<sup>†</sup> The analysis approximates the thermal conductivity as constant during the heating and cooling process.

## Comparing simulation and experiment

Simulated temperature–time curves of the laser heated zeolites were generated using the best-estimate values for the simulation input parameters at each temperature. Additional simulations were carried out to establish the maximum and minimum T-jumps possible within the degree of uncertainty in the input parameters, and these were used to generate the error bars of the reported simulation results.

Fig. 8 shows both the simulated and experimentally derived temperature profiles for a T-jump from 175 °C  $T_{\text{Act}}$  as an example. It can be seen that the experimental results correspond closely with those derived from the simulation, with the maximum experimental  $\Delta T$  of 89 °C being 85% of that predicted by the simulation. The uncertainties in the input parameters gave an error bar in the simulated  $\Delta T$  of  $\pm 40$  °C, however the close agreement with the experimental results indicates that the best-estimate input parameters are realistic.

In the simulations, increasing  $T_{\text{Init}}$  had the effect of increasing the zeolite specific heat capacity and removing water from the sample, decreasing the sample absorbance in the laser-pumped OH stretch region of 3600  $\text{cm}^{-1}$ . These changes result in the simulated T-jump magnitude diminishing with increased starting temperature. Fig. 9 compares the T-jump magnitude,  $\Delta T$ , achieved at each temperature in both the experimental and simulated datasets. The reduction in simulated and experimental  $\Delta T$  with increased temperature is readily

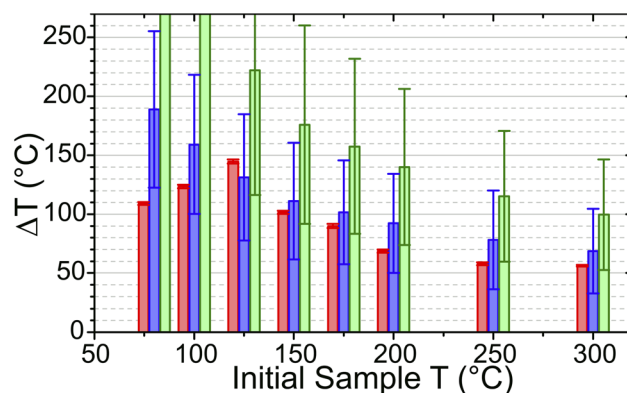


Fig. 9 Average temperature jump measured between  $10^{-8}$  and  $10^{-5}$  s as determined by: experiment based on changes in silanol mode intensity (red); heat transfer simulations (blue); energy absorption calculations (green). Error bars for simulation and calculation values are based on the uncertainties in the input parameters.

apparent. It can be concluded that the variation in pump absorbance of the zeolite sample has the greatest effect on T-jump magnitude  $\Delta T$  variation with start temperature, with changes in heat capacity being small enough in this temperature range that they are of secondary importance.

As an alternative to the simulations described above, a simple way of computing  $\Delta T$  is to simply consider the amount of energy  $E_{\text{pump}}$  absorbed by the sample of density  $\rho$  and optical density OD in a volume ( $V$ ) defined by the beam waist and pathlength:<sup>44</sup>

$$\Delta T = \frac{E_{\text{pump}} \text{OD}}{\rho V C_p} \quad (3)$$

ESI, Section 18<sup>†</sup> describes the estimation of heated volume,  $V$ . Temperature jumps computed from eqn (3) are shown in Fig. 9 and overestimate the value of  $\Delta T$  at all temperatures, reflective of the fact that this represents the maximum achievable T-jump magnitude without considering the weighting of the measured temperature due to the profile of the probe beam, inhomogeneous distribution of the pump beam energy, or the effect of evolution of the sample heat capacity over the course of the laser heating cycle.

Water uptake *via* the formation of water clusters in ZSM-5 at temperatures below 125 °C will increase the heat capacity of the zeolite sample. This is not accounted for in either set of simulated  $\Delta T_{\text{Max}}$  values, which continue to increase with decreasing temperature down to the lowest temperature measured. In contrast, the experimental temperature jump magnitudes diminish at these lower temperatures. An estimate of the zeolite heat capacity ( $C_p$ ) from experimental  $\Delta T$  values can be obtained through use of eqn (3) (with details of this calculation given in ESI Section 18<sup>†</sup>). These estimated  $C_p$  values match those from Lu *et al.*<sup>40</sup> used in the simulations at  $T \geq 125$  °C (Fig. 10). At lower temperatures, these estimates are up to 250% of the value predicted for the zeolite alone, indicating that water clusters within the zeolite raise the heat capacity of the sample. That the

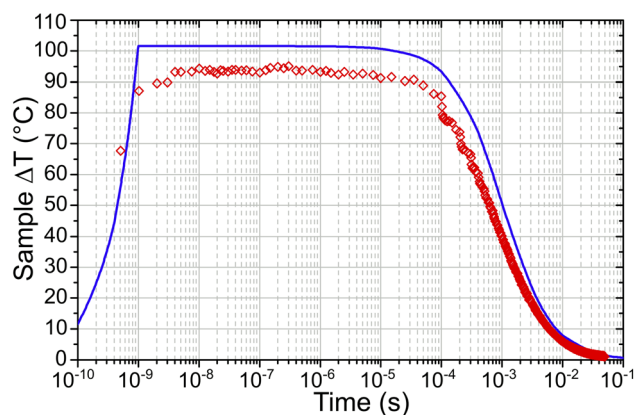


Fig. 8 Average sample temperature across the probed region vs. time for a temperature jump from 175 °C  $T_{\text{Act}}$  as determined experimentally (red) and from simulations (blue). The simulation uses the best estimates for input parameters.

difference in predicted and experimentally-estimated  $C_p$  values is so large suggests that this difference in heat capacities is likely to be responsible for the majority of the deviation from simulated heating behaviour observed experimentally below 125 °C.

We now return to the bi-exponential cooling of the zeolite samples observed experimentally. The simulated sample cooling was also found to be bi-exponential regardless of the value of thermal conductivity used, with only the magnitude of the time constants varying with  $\kappa$ . Fit parameters are reported in the ESI, Section 10.† The  $\tau_1:\tau_2$  ratio and  $A_1/A_2$  for a given start temperature were the same, whether averaged over the FWHM diameter of the probe beam, or at different single-positions in the sample. The simulations therefore indicate that the bi-exponential cooling is not a consequence of averaging the temperature over the probed region of the sample. Although both cooling processes are slowed by the presence of water clusters,  $\tau_2$  is more strongly affected, leading to the  $\tau_2/\tau_1$  ratio being proportional to the level of water clusters at low temperatures. The neglect of the properties of water from the simulation explains the inability to match the simulated cooling to experimental results at temperatures  $\leq 125$  °C.

By carrying out a series of laser heating simulations of different heat distributions within the zeolite (described in the ESI, Section 19†), the bi-exponential nature of the sample cooling was found to be phenomenologically due to redistribution of the inhomogeneous thermal energy profile within the heated region of the zeolite. Newton's single exponential law of cooling assumes that heat redistribution within the heated region is much faster than the overall cooling, either due to the volume of the heated region being insignificant or the thermal conductivity ( $\kappa$ ) of the heated region being higher than the surroundings into which it cools.<sup>45–48</sup> The laser-pumped sample volume is large enough for an inhomogeneous heat distribution to be present immediately post-pumping. Cooling occurs primarily through conduction into the surrounding, cooler zeolite, whose  $\kappa$  value differs minimally from that in the heated

region. Redistribution of the thermal profile in the heated region and cooling into the unheated zeolite therefore occur on similar timescales resulting in bi-exponential cooling. Increasing the degree of inhomogeneity in the sample heating has the effect of increasing the relative contribution of the 'slow'  $\tau_2$  term to the overall cooling curve. In the experimental data, the inhomogeneous temperature distribution arises from the Gaussian, divergent nature of the pump beam and the ratio of  $\kappa$  between the pumped and unpumped regions. The relative contribution of the  $\tau_2$  term is essentially constant for all  $T_{\text{init}}$  values ( $A_2 = 0.33 \pm 0.02$ ). This implies that in the bi-exponential cooling, the 'fast' term represents the overall cooling while the 'slow' term represents the thermal energy redistribution.

## Multiple-pulse heating

While the results reported above show that significant T-jumps are achievable with a single pump pulse, even larger heating magnitudes are possible by changing the pump trigger to initiate a variable-length burst of pump pulses at 1 kHz, pumping the sample repeatedly in quick succession. This approach has similarities to the modulated CW laser heating method reported for solution studies by Ashwood, *et al.*,<sup>15</sup> but retains nanosecond time resolution and direct excitation of fundamental modes. Fig. 11 compares the sample heating in a single-pulse heating experiment on HOD in ZSM-5 at  $T_{\text{init}} = 125$  °C with the same sample pumped with a 25-pulse burst. This experiment was performed with the pump OPO set at a wavelength of 2.9  $\mu\text{m}$  rather than the 2.8  $\mu\text{m}$  used in the results reported above, an area of the sample IR spectrum with lower absorbance, explaining the smaller single-pulse T-jumps achieved compared with Fig. 6.

As shown in Fig. 11(a) for 1 kHz burst pumping of ZSM-5, the second and subsequent pulses arrive before the sample fully cools, meaning that each subsequent pulse heats the sample to higher temperatures. Over the sequence of pump pulses, although the heating reduces as water is desorbed from the sample (which reduces the pump absorbance), heating continues throughout the burst. The rate of temperature gain per pump pulse becomes constant once the sample reaches a fully-desorbed state at *ca.* 200 °C, which is after pulse # 10 ( $\Delta T \sim 80$  °C). This means that arbitrarily large T-jumps may be achieved in zeolite samples through use of a sufficiently long pump burst, subject to the maximum repetition rate of the pump laser. Computer simulations indicate that for the setup in Fig. 1, T-jumps as large as 350 °C above starting temperature can be achieved with a 50-pulse burst, as shown in the ESI, Section 20.†

Use of TRMPS probing means that it is possible to observe each individual T-jump in the pump burst with nanosecond time resolution, allowing the evolution of the sample to be observed at each successive temperature caused by each laser pulse of the burst (Fig. 11(b)). Fitting of the sample cooling kinetics for each pulse shows the fast bi-exponential decay constant increasing from *ca.* 1 to *ca.* 3 ms over the course of the burst process. This can be attributed to the heated volume of the sample enlarging with the repeated laser pulses relative to the laser-pumped volume. Simulations indicate that the full-

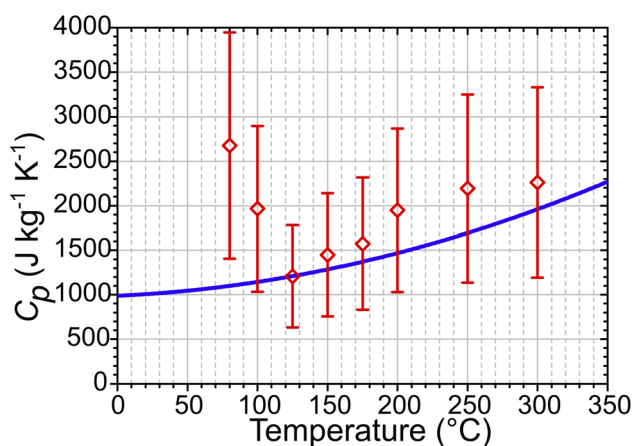


Fig. 10 Zeolite  $C_p$  values calculated from experimental T-jump data using eqn (3) (red) compared to simulation input  $C_p$  values derived from ref. 40 (blue).





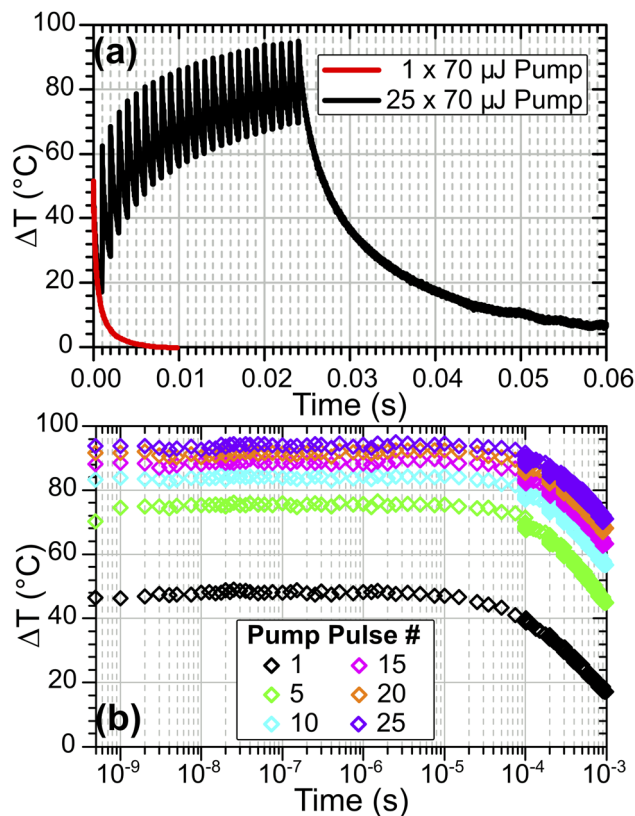


Fig. 11 (a) Sample temperature evolution for HOD/H<sub>2</sub>O in ZSM-5 at  $T_{\text{init}} = 125$  °C following pumping by 1× (red) and 25× (black) 70 μJ pump pulses. (b) Comparison of temperature evolution in first 1 ms following indicated pulse number in 25-pulse burst showing nanosecond time resolution throughout full range.

width at half maximum of the radial temperature distribution increases from 36 μm after a single pulse to *ca.* 80 μm after a 50-pulse burst (ESI, Section 20†). The subsequent reduction in thermal gradient in the radial direction leads to slower cooling.

## Conclusions

Pulsed-laser heating with time-resolved multiple probe infrared absorption spectroscopy and tightly focussed pump and probe beams has been applied to induce and study T-jumps in nanoporous zeolite catalysts. The single-shot temperature jumps achieved are 5× larger than those previously described for time-resolved heating studies in solution<sup>14,15</sup> and enable the possibility of using pulsed laser heating to selectively activate and study heterogeneous catalytic activity in reactive systems.

The magnitude of T-jumps in partially hydrated zeolite systems were measured through the use of temperature-related changes in the positioning of the  $\nu(\text{SiOD})$  silanol mode. This allows us to determine that our approach is able to produce T-jumps of  $\geq 50$  °C from a pump energy input of 70 μJ in the bare zeolite. Even larger temperature changes are achievable at temperatures where the sample contains adsorbed water, increasing absorption of the pump laser light. Use of multiple-pulse pumping allows temperature jumps to be extended to achieve arbitrarily large increases in temperature while still

providing nanosecond-resolution information on the sample after each pulse of the burst.

The rate of cooling of the ZSM-5 sample studied was unaffected by starting temperature in cases where the sample contained  $\leq 1$  water molecule per acid site and resulted in the sample remaining at least 10 °C above base temperature for  $>1$  ms in all cases. Owing to the increased presence of water clusters, low starting temperatures show decreased T-jump magnitude and slower recovery. One particular feature of interest is the weaker than expected appearance of free Brønsted site in the transient infrared data upon loss of hydrogen bonded Brønsted site. Further tests will be required to determine whether this is due to laser induced deprotonation of the Brønsted site, as suggested by the data.

Using fundamental zeolite properties, laser beam properties and IR absorption of the sample, two-dimensional heat transfer modelling accurately describes the experimental results with respect to both  $\Delta T$  and bi-exponential cooling rate, whilst also providing information on the heat distribution within the sample. The close agreement with experimental results supports its use as an approach for investigating T-jumps in zeolite/adsorbate systems which do not have convenient modes for spectroscopic determination of the magnitude of  $\Delta T$ . Simulated  $\Delta T$  values for such systems can be calibrated using ZSM-5 as a reference system to derive a correction factor accounting for parameters difficult to determine accurately, such as pump-probe overlap.

The method of T-jump spectroscopy described here can be applied to other zeolite materials, provided that they have suitable optical density and thickness. Use of the silanol thermometer method to evaluate the temperature changes in the sample requires that any adsorbates do not interact strongly with the silanol group, as this will disturb the linear dependence of the  $\nu(\text{SiOD})$  mode on sample temperature. For a given zeolite, the  $\Delta T$  achieved and cooling rate of the excited sample varies according to the  $C_p$ ,  $\kappa$  and pump absorbance. These are the primary properties influencing the T-jump behaviour. Reported  $C_p$  and  $\kappa$  values of different zeolites have been observed to vary by up to  $\pm 70\%$ ,<sup>40,49</sup> indicating that single pulse laser heating of 35 to 210 °C is possible using the approach reported here.

## Data availability

Data available on reasonable request.

## Author contributions

Alexander Hawkins (investigation, writing – original draft), Amy Edmeades (investigation, software, writing – original draft), Christopher Hutchison (investigation), Michael Towrie (investigation, writing – review and editing), Russell Howe (investigation, writing – review and editing), Greg Greetham (investigation, writing – review and editing), Paul Donaldson (investigation, writing – review and editing, project administration, funding acquisition).

## Conflicts of interest

There are no conflicts to declare.



## Acknowledgements

This work was supported by a UKRI Future Leaders Fellowship grant (MR/S015574/1, MR/X011119/1). The Science and Technology Facilities Council is thanked for funded access to the ULTRA laboratories of the CLF (CLF-Ultra programme access LSF1828). The authors are grateful to the Research Complex at Harwell for lab-space and support.

## Notes and references

- 1 A. Corma, Inorganic Solid Acids and Their Use in Acid-Catalyzed Hydrocarbon Reactions, *Chem. Rev.*, 1995, **95**(3), 559–614.
- 2 E. Pérez-Botella, S. Valencia and F. Rey, Zeolites in Adsorption Processes: State of the Art and Future Prospects, *Chem. Rev.*, 2022, **122**(24), 17647–17695.
- 3 Q. Zhang, S. Gao and J. Yu, Metal Sites in Zeolites: Synthesis, Characterization, and Catalysis, *Chem. Rev.*, 2023, **123**(9), 6039–6106.
- 4 A. J. Orr-Ewing, Taking the Plunge: Chemical Reaction Dynamics in Liquids, *Chem. Soc. Rev.*, 2017, **46**(24), 7597–7614.
- 5 P. M. Donaldson, G. M. Greetham, C. T. Middleton, B. M. Luther, M. T. Zanni, P. Hamm and A. T. Krummel, Breaking Barriers in Ultrafast Spectroscopy and Imaging Using 100 kHz Amplified Yb-Laser Systems, *Acc. Chem. Res.*, 2023, **56**(15), 2062–2071.
- 6 L. A. Hammarback, J. B. Eastwood, T. J. Burden, C. J. Pearce, I. P. Clark, M. Towrie, A. Robinson, I. J. S. Fairlamb and J. M. Lynam, A Comprehensive Understanding of Carbon–Carbon Bond Formation by Alkyne Migratory Insertion into Manganacycles, *Chem. Sci.*, 2022, **13**(34), 9902–9913.
- 7 A. Šrut, S. Mai, I. V. Sazanovich, J. Heyda, A. Vlček, L. González and S. Zálaiš, Nonadiabatic Excited-State Dynamics of  $\text{ReCl}(\text{CO})_3(\text{Bpy})$  in Two Different Solvents, *Phys. Chem. Chem. Phys.*, 2022, **24**(42), 25864–25877.
- 8 P. M. Keane, C. Zehe, F. E. Poynton, S. A. Bright, S. Estayalo-Adrián, S. J. Devereux, P. M. Donaldson, I. V. Sazanovich, M. Towrie, S. W. Botchway, C. J. Cardin, D. C. Williams, T. Gunnlaugsson, C. Long, J. M. Kelly and S. J. Quinn, Time-Resolved Infra-Red Studies of Photo-Excited Porphyrins in the Presence of Nucleic Acids and in HeLa Tumour Cells: Insights into Binding Site and Electron Transfer Dynamics, *Phys. Chem. Chem. Phys.*, 2022, **24**(44), 27524–27531.
- 9 M. Sneha, G. L. Thornton, L. Lewis-Borrell, A. S. H. Ryder, S. G. Espley, I. P. Clark, A. J. Cresswell, M. N. Grayson and A. Orr-Ewing, J. Photoredox-HAT Catalysis for Primary Amine  $\alpha$ -C–H Alkylation: Mechanistic Insight with Transient Absorption Spectroscopy, *ACS Catal.*, 2023, **13**(12), 8004–8013.
- 10 C. M. Phillips, Y. Mizutani and R. M. Hochstrasser, Ultrafast Thermally Induced Unfolding of RNase A, *Proc. Natl. Acad. Sci. U.S.A.*, 1995, **92**(16), 7292–7296.
- 11 R. H. Callender, R. B. Dyer, R. Gilmanshin and W. H. Woodruff, Fast Events in Protein Folding: The Time Evolution of Primary Processes, *Annu. Rev. Phys. Chem.*, 1998, **49**, 173–202.
- 12 H. S. Chung, M. Khalil, A. W. Smith, Z. Ganim and A. Tokmakoff, Conformational Changes during the Nanosecond-to-Millisecond Unfolding of Ubiquitin, *Proc. Natl. Acad. Sci. U.S.A.*, 2005, **102**(3), 612–617.
- 13 K. Hauser, C. Krejtschi, R. Huang, L. Wu and T. A. Keiderling, Site-Specific Relaxation Kinetics of a Tryptophan Zipper Hairpin Peptide Using Temperature-Jump IR Spectroscopy and Isotopic Labeling, *J. Am. Chem. Soc.*, 2008, **130**(10), 2984–2992.
- 14 G. M. Greetham, I. P. Clark, B. Young, R. Fritsch, L. Minnes, N. T. Hunt and M. Towrie, Time-Resolved Temperature-Jump Infrared Spectroscopy at a High Repetition Rate, *Appl. Spectrosc.*, 2020, **74**(6), 720–727.
- 15 B. Ashwood, N. H. C. Lewis, P. J. Sanstead and A. Tokmakoff, Temperature-Jump 2D IR Spectroscopy with Intensity-Modulated CW Optical Heating, *J. Phys. Chem. B*, 2020, **124**(39), 8665–8677.
- 16 C. P. Howe, G. M. Greetham, B. Procacci, A. W. Parker and N. T. Hunt, Sequence-Dependent Melting and Refolding Dynamics of RNA UNCG Tetraloops Using Temperature-Jump/Drop Infrared Spectroscopy, *J. Phys. Chem. B*, 2023, **127**(7), 1586–1597.
- 17 H. Hoffmann, E. Yeager and J. Stuehr, Laser Temperature-Jump Apparatus for Relaxation Studies in Electrolytic Solutions, *Rev. Sci. Instrum.*, 2003, **39**(5), 649–653.
- 18 H. S. Chung, M. Khalil, A. W. Smith and A. Tokmakoff, Transient Two-Dimensional IR Spectrometer for Probing Nanosecond Temperature-Jump Kinetics, *Rev. Sci. Instrum.*, 2007, **78**(6), 063101.
- 19 J. Kubelka, Time-Resolved Methods in Biophysics. 9. Laser Temperature-Jump Methods for Investigating Biomolecular Dynamics, *Photochem. Photobiol. Sci.*, 2009, **8**(4), 499–512.
- 20 S. D. Hellring and G. J. Green, Laser-Induced Thermal Desorption (LITD) from Zeolites: Apparatus and Technique for Rapid, in Vacuo Sample Desorption for FTi.r. Analysis, *Zeolites*, 1994, **14**(1), 3–6.
- 21 H. Ernst, D. Freude, T. Mildner and I. Wolf, Laser-Supported High-Temperature MAS NMR for Time-Resolved in Situ Studies of Reaction Steps in Heterogeneous Catalysis, *Solid State Nucl. Magn. Reson.*, 1996, **6**(2), 147–156.
- 22 P. M. Allotta and P. C. Stair, Time-Resolved Studies of Ethylene and Propylene Reactions in Zeolite H-MFI by In-Situ Fast IR Heating and UV Raman Spectroscopy, *ACS Catal.*, 2012, **2**(11), 2424–2432.
- 23 M. Bonn, M. J. P. Brugmans, A. W. Kleyn and R. A. van Santen, Fast Energy Delocalization upon Vibrational Relaxation of a Deuterated Zeolite Surface Hydroxyl, *J. Chem. Phys.*, 1995, **102**(5), 2181–2186.
- 24 M. J. P. Brugmans, M. Bonn, H. J. Bakker and A. Lagendijk, Multiphonon Decay of Stretch Vibrations in Zeolites, *Chem. Phys.*, 1995, **201**(1), 215–225.
- 25 P. M. Donaldson, R. F. Howe, A. P. Hawkins, M. Towrie and G. M. Greetham, Ultrafast 2D-IR Spectroscopy of Intensely



- Optically Scattering Pelleted Solid Catalysts, *J. Chem. Phys.*, 2023, **158**(11), 114201.
- 26 G. M. Greetham, D. Sole, I. P. Clark, A. W. Parker, M. R. Pollard and M. Towrie, Time-Resolved Multiple Probe Spectroscopy, *Rev. Sci. Instrum.*, 2012, **83**(10), 103107.
- 27 Y. Feng, I. Vinogradov and N.-H. Ge, General Noise Suppression Scheme with Reference Detection in Heterodyne Nonlinear Spectroscopy, *Opt. Express.*, 2017, **25**(21), 26262–26279.
- 28 A. Zecchina, F. Geobaldo, G. Spoto, S. Bordiga, G. Ricchiardi, R. Buzzoni and G. Petrini, FTIR Investigation of the Formation of Neutral and Ionic Hydrogen-Bonded Complexes by Interaction of H-ZSM-5 and H-Mordenite with CH<sub>3</sub>CN and H<sub>2</sub>O: Comparison with the H-NAFION Superacidic System, *J. Phys. Chem.*, 1996, **100**(41), 16584–16599.
- 29 J. N. Kondo, M. Iizuka, K. Domen and F. Wakabayashi, IR Study of H<sub>2</sub>O Adsorbed on H-ZSM-5, *Langmuir*, 1997, **13**(4), 747–750.
- 30 S. Bordiga, C. Lamberti, F. Bonino, A. Travert and F. Thibault-Starzyk, Probing Zeolites by Vibrational Spectroscopies, *Chem. Soc. Rev.*, 2015, **44**(20), 7262–7341.
- 31 J. H. Hack, X. Ma, Y. Chen, J. P. Dombrowski, N. H. C. Lewis, C. Li, H. H. Kung, G. A. Voth and A. Tokmakoff, Proton Dissociation and Delocalization under Stepwise Hydration of Zeolite HZSM-5, *J. Phys. Chem. C*, 2023, **127**(32), 16175–16186.
- 32 M. F. Claydon and N. Sheppard, The Nature of “A,B,C”-Type Infrared Spectra of Strongly Hydrogen-Bonded Systems; Pseudo-Maxima in Vibrational Spectra, *J. Chem. Soc. D*, 1969, **23**, 1431–1433.
- 33 A. G. Pelmenschikov and R. A. van Santen, Water Adsorption on Zeolites: Ab-Initio Interpretation of IR Data, *J. Phys. Chem.*, 1993, **97**(41), 10678–10680.
- 34 A. Vjunov, M. Wang, N. Govind, T. Huthwelker, H. Shi, D. Mei, J. L. Fulton and J. A. Lercher, Tracking the Chemical Transformations at the Brønsted Acid Site upon Water-Induced Deprotonation in a Zeolite Pore, *Chem. Mater.*, 2017, **29**(21), 9030–9042.
- 35 S. M. Campbell, D. M. Bibby, J. M. Coddington, R. F. Howe and R. H. Meinhold, Dealumination of HZSM-5 Zeolites: I. Calcination and Hydrothermal Treatment, *J. Catal.*, 1996, **161**(1), 338–349.
- 36 S. M. Campbell, X. Z. Jiang and R. F. Howe, Methanol to Hydrocarbons: Spectroscopic Studies and the Significance of Extra-Framework Aluminium, *Microporous Mesoporous Mater.*, 1999, **29**(1–2), 91–108.
- 37 M. Niwa, K. Suzuki, N. Katada, T. Kanougi and T. Atoguchi, Ammonia IRMS-TPD Study on the Distribution of Acid Sites in Mordenite, *J. Phys. Chem. B*, 2005, **109**(40), 18749–18757.
- 38 M. Niwa, K. Suzuki, K. Isamoto and N. Katada, Identification and Measurements of Strong Brønsted Acid Site in Ultrastable Y (USY) Zeolite, *J. Phys. Chem. B*, 2006, **110**(1), 264–269.
- 39 *Mathematica*, Wolfram Research, Inc., 2022.
- 40 X. Lu, Y. Wang, L. Estel, N. Kumar, H. Grénman and S. Leveneur, Evolution of Specific Heat Capacity with Temperature for Typical Supports Used for Heterogeneous Catalysts, *Processes*, 2020, **8**(8), 911.
- 41 A. M. Greenstein, S. Graham, Y. C. Hudiono and S. Nair, Thermal Properties and Lattice Dynamics of Polycrystalline MFI Zeolite Films, *Nanoscale Microscale Thermophys. Eng.*, 2006, **10**(4), 321–331.
- 42 T. Coquil, C. M. Lew, Y. Yan and L. Pilon, Thermal Conductivity of Pure Silica MEL and MFI Zeolite Thin Films, *J. Appl. Phys.*, 2010, **108**(4), 044902.
- 43 J. Fang, Y. Huang, C. M. Lew, Y. Yan and L. Pilon, Temperature Dependent Thermal Conductivity of Pure Silica MEL and MFI Zeolite Thin Films, *J. Appl. Phys.*, 2012, **111**(5), 054910.
- 44 K. C. Robben, Improvements in the Sensitivity of 2D IR Measurements by Edge-Pixel Referencing, Model Fitting, and Signal Enhancement Methods, *PhD thesis*, The University of Iowa, United States – Iowa, 2022.
- 45 S. L. E. F. da Silva, Newton's Cooling Law in Generalised Statistical Mechanics, *Physica A Stat. Mech. Appl.*, 2021, **565**, 125539.
- 46 A. Mondol, R. Gupta, S. Das and T. Dutta, An Insight into Newton's Cooling Law Using Fractional Calculus, *J. Appl. Phys.*, 2018, **123**(6), 064901.
- 47 A. Brown and T. K. Marshall, Body Temperature as a Means of Estimating the Time of Death, *Forensic Sci.*, 1974, **4**, 125–133.
- 48 M. I. Davidzon, Newton's Law of Cooling and Its Interpretation, *Int. J. Heat Mass Transf.*, 2012, **55**(21), 5397–5402.
- 49 S. K. Schnell and T. J. H. Vlugt, Thermal Conductivity in Zeolites Studied by Non-Equilibrium Molecular Dynamics Simulations, *Int. J. Thermophys.*, 2013, **34**(7), 1197–1213.

